Geophysical Research Letters

RESEARCH LETTER
10.1029/2022GL099017

Summer Midlatitude Stationary Wave Patterns Synchronize Northern Hemisphere Wildfire Occurrence

Hien X. Bui[1,2,3], Axel Timmermann[2,3], June-Yi Lee[2,3,4], Eric D. Maloney[5], Yi-Xian Li[6], Ji-Eun Kim[2,3], Jacquelyn Shuman[7], Sun-Seon Lee[2,3], and William R. Wieder[7,8]

[1]ARC Centre of Excellence for Climate Extremes, School of Earth, Atmosphere and Environment, Monash University, Clayton, VIC, Australia, [2]Center for Climate Physics, Institute for Basic Science, Busan, South Korea, [3]Pusan National University, Busan, South Korea, [4]Research Center for Climate Sciences, Pusan National University, Busan, South Korea, [5]Department of Atmospheric Science, Colorado State University, Fort Collins, CO, USA, [6]Department of Atmospheric Sciences, National Central University, Taoyuan, Taiwan, [7]Climate and Global Dynamics Laboratory, National Center for Atmospheric Research, Boulder, CO, USA, [8]Institute of Arctic and Alpine Research, University of Colorado, Boulder, CO, USA

Abstract Midlatitude stationary waves are relatively persistent large-scale longitudinal variations in atmospheric circulation. Although recent case studies have suggested a close connection between stationary waves and extreme weather events, little is known about the global-scale linkage between stationary waves and wildfire activity, as well as the potential changes in this relationship in a warmer climate. Here, by analyzing the Community Earth System Model version 2 large ensemble, we show that a zonal wavenumber 5–6 stationary wave pattern tends to synchronize wildfire occurrences across the Northern Hemisphere midlatitudes. The alternation of upper-troposphere ridges and troughs creates a hemispheric-scale spatial pattern of alternating hot/dry and cold/wet conditions, which increases or decreases wildfire occurrence, respectively. More persistent high-pressure conditions drastically increase wildfire probabilities. Even though the dynamics of these waves change little in response to anthropogenic global warming, the corresponding midlatitude wildfire variability is projected to intensify due to changes in climate background conditions.

Plain Language Summary Wildfires are natural disasters that often cause severe public emergencies. Increasing our ability to predict wildfire occurrence has the potential to reduce the loss of life and property associated with them. In this study, we analyze new large-ensemble simulations conducted with the Community Earth System Model, version 2 in 1 degree resolution to elucidate the linkage between atmospheric stationary waves and clustered Northern Hemisphere wildfire occurrences, as well as the potential changes in this relationship in a warmer climate. Our analysis shows that wildfire occurrences tend to be clustered regionally by a zonal wavenumber 5–6 stationary wave pattern. More persistent regional high-pressure conditions further increase wildfire probabilities. This relationship can be largely explained by the quasi-stationary moisture and relative humidity conditions which are associated with the summer midlatitude wave trains. More persistent regional high-pressure conditions further increase likelihood of wildfire occurrences.

Key Points:

- Simulations from the CESM2-LE are used to examine the linkage between atmospheric stationary waves and Northern Hemisphere wildfire
- Wildfire occurrences tend to be clustered regionally and temporally by a zonal wavenumber 5–6 stationary wave pattern
- More persistent regional high-pressure conditions further increase wildfire probabilities

Supporting Information:

Supporting Information may be found in the online version of this article.

Correspondence to:

H. X. Bui and J.-Y. Lee,
hien.bui@monash.edu;
juneyi@pusan.ac.kr

Citation:

Bui, H. X., Timmermann, A., Lee, J.-Y., Maloney, E. D., Li, Y.-X., Kim, J.-E., et al. (2022). Summer midlatitude stationary wave patterns synchronize Northern Hemisphere wildfire occurrence. *Geophysical Research Letters*, *49*, e2022GL099017. https://doi.org/10.1029/2022GL099017

Received 3 APR 2022
Accepted 12 SEP 2022

1. Introduction

Wildfire is a natural disaster and a matter of public emergency worldwide (Shukla et al., 2019). The 2018 wildfire season was a record-setting year of wildfires, including the 2018 Camp Fire that was the deadliest and most destructive recorded wildfire with more than 80 deaths and a cost of over 16 billion USD in California (Schulze et al., 2020). In Greece, a series of wildfires during the 2018 European heatwave event also claimed over 100 lives (Lagouvardos et al., 2018). The largest recorded wildfire that occurred in the past century – the 2003 Russia wildfire – produced a 200,000 km^2 burned area (Edwards et al., 2004). The climatological May to October Northern Hemisphere (NH) fire season is associated with dry conditions and less soil moisture that make wildfire more likely to occur (Brey et al., 2021). Increasing our capability for predicting wildfire occurrences has the potential to reduce the loss of life and property associated with them.

Midlatitude stationary waves are characterized by a planetary-scale longitudinal variation in the atmospheric circulation that is relatively invariable on weekly to seasonal timescales, also known as circumglobal teleconnection (CGT; Branstator, 2002; Nakamura et al., 1997; Wills et al., 2019). These disturbances are characterized

by an upper-troposphere ridge/trough pattern, accompanied by high/low-pressure anomalies at the surface, that develops and moves slowly (i.e., is quasi-stationary) around the globe. Wave patterns can be amplified through interactions with topography, surface conditions, and other atmospheric phenomena (Held et al., 2002), creating so-called (quasi)resonant conditions that may be linked to extreme weather events (Coumou et al., 2014; Petoukhov et al., 2013). Recent studies have shown that some wave patterns related to the jet stream, characterized by a zonal wavenumber 5–7, are also linked to severe heatwaves (see Kornhuber et al., 2019, 2020). Although still under debate in the field of Rossby wave dynamics (e.g., Wirth & Polster, 2021), such unusual persistent wave trains cause hemispherically-organized patterns of drying and warming, as well as wetting and cooling conditions, which can provide more or less favorable environments on wildfire occurrences.

Previous studies have focused on the persistent anomalous high pressure atmospheric conditions – associated with midlatitude stationary waves – that can increase fire occurrences in specific regions, such as the Mediterranean (Ruffault et al., 2020) or Canada (Petoukhov et al., 2018), among many others (e.g., Conard & Ponomarev, 2020; Teng et al., 2013; Valendik et al., 2014; Wolf et al., 2018). However, little is known about whether hemispheric-scale atmospheric disturbances can synchronize the occurrence of wildfires across the NH. Here we will elucidate the linkage between large-scale midlatitude stationary waves in boreal summer and the extended coherent anomalous patterns of wildfire occurrences across Europe, Asia and North America; the potential changes in this relationship in a warmer climate will also be discussed.

2. Data and Methodology

2.1. Data

We examine the impacts of stationary waves on wildfire activity using simulations from the National Center for Atmospheric Research (NCAR) Community Earth System Model version 2 large ensemble with a horizontal resolution of 0.9°×1.25° (CESM2-LE; Rodgers et al., 2021). Using a large ensemble with different initial conditions not only increases the data volume that allows us to better characterize the entire distribution of climate variability, but also creates an improved characterization of the seasonal cycle and complex long-term trends (Haugen et al., 2018). As a result, atmosphere-land processes in the model produced by internal variability can be readily identified in the large ensemble simulations.

The fire data, including fire count and burned area, are output from Community Land Model version 5 (CLM5; Lawrence et al., 2019) and atmospheric conditions are from Community Atmospheric Model version 6 (CAM6; Danabasoglu et al., 2020). The CLM5 uses a fire parameterization that includes the effects of climate and weather conditions, vegetation composition and canopy height, and human activity (Li & Lawrence, 2017). The last 50 ensemble members forced by CMIP6 protocols with smoothed biomass burning emissions were analyzed in the current study. As we focus on the NH midlatitude boreal summer, only data during extended boreal summer (May–October) were analyzed. Daily mean fields during the historical forcing period of 1981–2010 (HIST) are used to assess fire activity in the current climate and are compared with the 2071–2100 period in shared socioeconomic pathways (SSPs) with fossil-fueled development combined with a 7 W/m^2 forcing scenario (SSP370; O'Neill et al., 2016).

We also compared our fire data from the model with the observed fire emission data set from the Global Fire Emissions Database version 4 (GFED4; Giglio et al., 2013). The GFED4 combines satellite information on fire activity and vegetation productivity to estimate burned area and fire emissions. Admittedly, the observed fire emissions are governed not just area burned and/or fire counts but also by fuel load and fuel type, such as the vegetation burned by fire. In addition, the GFED4 daily emission data have limitations since they were obtained from redistributing monthly emissions with other fire information (van der Werf et al., 2017). Hence, our modeled fire counts or burned area could not be directly compared to fire emissions, and quantifying/validating of the model results is a topic of future work. Here, the daily fire emission data set from 2003 to 2020 was analyzed (Figure S1 in Supporting Information S1). The result shows qualitative similarities in the spatial distribution (although the detail structure, as might be expected, is noisy), suggesting that the basic spatial pattern and characteristics of the simulated wildfire dynamics are well-captured (e.g., Figure 1).

Given comments about the fire output from CLM5 in which parameterizations in both vegetation and fire components can influence various aspects of fire regimes (e.g., Hantson et al., 2020; Rabin et al., 2017), we also analyzed the fire weather index (Van Wagner & Pickett, 1985) calculated from the model to one taken from the

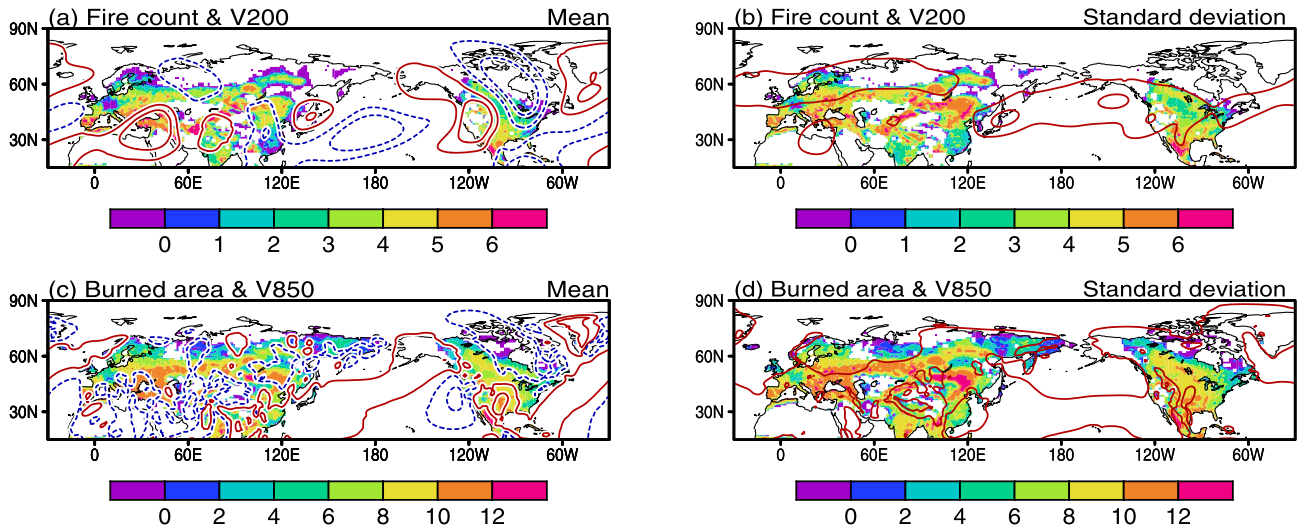

Figure 1. (a, b) Ensemble mean and standard deviation of fire count (shaded, units are count/year/100 km^2) and V200 (contour, units are m/s, with the first contour at 2 m/s and an interval of 2 m/s for the mean, and with the first contour at 6 m/s and an interval of 2 m/s for the standard deviation). (c, d) Similar to (a, b) but for burned area (shaded, units are 1,000 km^2/year) and V850 (contour, units are m/s, with the first contour at 1 m/s and an interval of 3 m/s for the mean, and with the first contour at 1 m/s and an interval of 2 m/s for the standard deviation) in historical simulation (1981–2010). Both fire count and burned area are shown with logarithmic color scale. Solid and dashed contours represent positive and negative values, respectively. Maps of other variables in the historical simulation and differences map between SSP370 (2071–2100) and historical (1981–2010) are shown in Supporting Information S1 (Figures S1–S3).

fifth global reanalysis produced by the European Center for Medium-Range Weather Forecasts (ERA5; Hersbach et al., 2020) during the same period of historical simulations (1981–2010) for comparison. The overall patterns are similar, indicating a consistency between the model and the reanalysis data (Figure S2 in Supporting Information S1), although the simulated amplitude appears to be smaller, which is probably related to the more frequent light rain bias in the model (Danabasoglu et al., 2020).

2.2. Methodology

The large-scale stationary wave metric is calculated as the deviation from the zonal mean of 200 hPa meridional wind (V200 hereafter). Note that the zonal mean of meridional wind is small especially along the jet, and the conclusions do not change without removing the zonal mean of meridional wind. A 15-day running mean is applied to V200 to remove high-frequency disturbances (Wills et al., 2019). We address the climatological mean and standard deviation of the stationary wave and wildfires by calculating the ensemble-wise mean and ensemble-wise standard deviation of the fields. This approach allows the examination of internal variability in the climate model (e.g., Haugen et al., 2018; Rodgers et al., 2021; Shaw & Voigt, 2015).

To examine the relationship between the stationary wave pattern and wildfire, we applied a singular value decomposition analysis (SVD; Wallace et al., 1992) to the daily anomaly data over the region from 25°–90°N, 0°–360°. Prior to performing the SVD analysis, the summer mean and long-term trend of the data in each ensemble member were removed by subtracting the ensemble mean from each ensemble member as has been done in Rodgers et al. (2021). The calculation is done for each ensemble member and for each period separately before the ensemble-wise average is done for 50 ensemble members. The multi-ensemble means SVD1 explains 23% of the total variance, suggesting the important contribution of stationary wave patterns to wildfire occurrence.

Finally, we also examine how consecutive high-pressure days impact wildfire activity. A high-pressure day is defined when omega at 500 hPa (ω500) is positive. Here we use ω500 to focus on the adiabatic process associated with vertical motion, and that there is a strong connection between ω500 and fire weather conditions (e.g., Davies et al., 2013; Rohini et al., 2016). Notably, under the sheared background westerlies, centers of anticyclone anomalies do not necessarily coincide with the those of descending motion, however our conclusions do not change as we focus on the persistence of the descending motion rather than intensity of a high-pressure system. Calculations are done at individual grid points and then averaged over the NH midlatitude (35°–70°N).

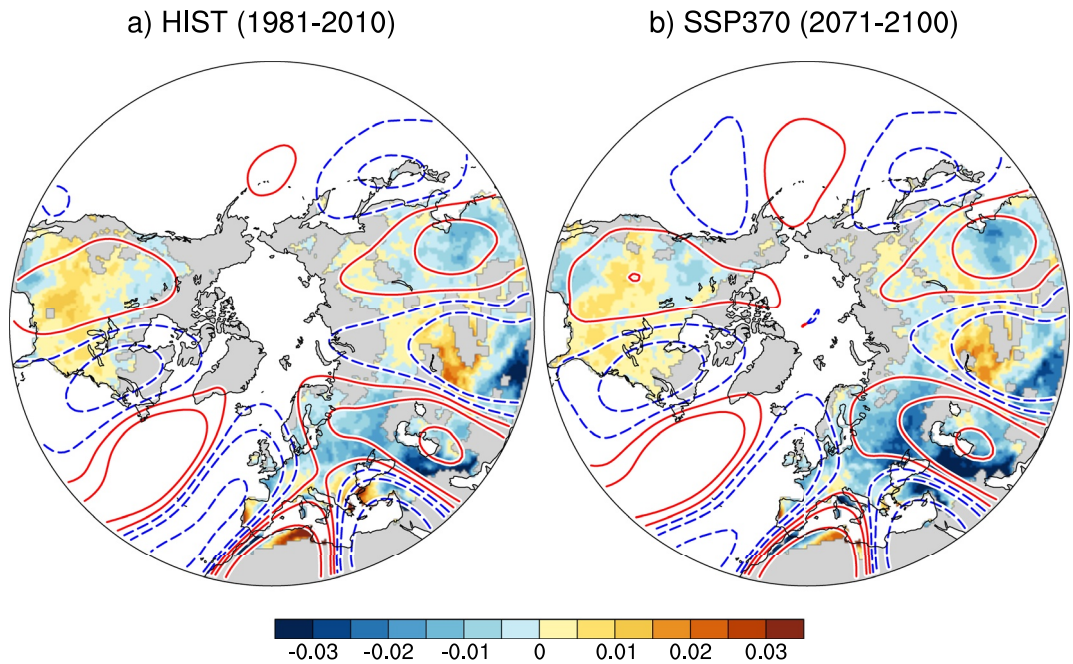

Figure 2. Maps of the first leading singular value decomposition (SVD) between daily anomaly of stationary waves (contour, solid and dashed contours represent positive and negative values, respectively, with the first contour at 1 and an interval of 2, no unit) and fire count (shaded, no unit, shaded gray represents the missing data) from the (a) historical (1981–2010) and (b) SSP370 (2071–2100) simulation. Maps of SVD analysis for North America and Eurasia separately are shown in Figures S4–S5 in Supporting Information S1.

3. Results

We first examine the connection between the climatological mean and the variability (i.e., standard deviation about the mean) of the NH stationary waves (c.f., contours in Figures 1a, 1c and Figures 1b, 1d). For the climatological mean, Figure 1a shows the upper-level anticyclone peaking over the Tibetan Plateau and Persian Gulf–associated with the South Asian monsoon, and upper-level troughs centered north of the Hawaiian Islands and east of the Caribbean Sea. The lower-level circulation (Figure 1c) shows a clear baroclinic wave pattern except over the North American continent that has a near barotropic wave pattern with a slight vertical tilt. For the variability (Figures 1b and 1d), the waves tend to occur over the mid-latitude region from 30° to 70°N, with a stronger intensity over the ocean rather than over land, which is quite different from its climatological mean.

We also compare the climatological mean and the variability of wildfire activity (c.f., shading in Figures 1a, 1c and Figures 1b, 1d). As shown, the increased mean wildfire activity in certain locations is primarily explained by the fact that low surface relative humidity and surface temperatures occur there (related to the evapotranspiration and land surface-air temperature relationship, e.g., Byrne & O'Gorman, 2015), associated with low precipitation and soil moisture (i.e., the vertically summed soil liquid water for veg land units only) (see also Figure S3 in Supporting Information S1). Similar to the climatological mean wildfire pattern, large variability in wildfires is found over Eurasia and North America (Figure 1b), suggesting that the variability of wildfire is strongly related to its climatological mean, which is common for positive definitive and highly skewed variables such as fire count.

3.1. Relationship Between the Stationary Wave Pattern and Wildfires

We now examine the relationship between stationary wave pattern and wildfire activity. To do this, a SVD analysis between V200 and fire counts in the NH midlatitude is conducted (Figure 2). The spatial pattern of V200 associated with the first SVD mode resembles a zonal wavenumber 5–6 structure in the midlatitude regions with high-pressure centered over the eastern United States, southern Europe, and northern Asia and low-pressure centers located in between (Figure 2a). This wave pattern is similar to the CGT pattern that dominates the Northern Hemisphere during boreal summer (e.g., Branstator, 2002; Ding & Wang, 2005). The fire count anomalies

associated with the leading SVD show a correspondence with this wave pattern: regions with positive fire anomalies are generally collocated with the surface high-pressure center (i.e., east side of the upper-tropospheric ridge), while regions with negative fire anomalies are collocated with the surface low-pressure center (i.e., east side of the upper-tropospheric trough). This behavior is especially apparent when the SVD is applied between the regional fire domain (e.g., central and eastern Eurasian continent) and the NH V200 (see Figure S4 in Supporting Information S1). However, we note that the pattern is not as clear over North America (Figure S5 in Supporting Information S1) and the western Eurasian continent, which may be related to a more barotropic mean structure over the region and thus deserves further analysis. In fact, large-scale conditions conducive for wildfire activity over the North America are complicated as it has been reported in previous studies that conditions favorable for fire on the U.S. West Coast are associated with a ridge aloft, while on the U.S. Great Plains they are not (Crimmins, 2006; Lindley et al., 2017). Nevertheless, the results show that wildfires in the midlatitude region tend to be spatially organized by a zonal wavenumber 5–6 stationary wave pattern. In a warmer climate by the end of the 21st century (2071–2100), the wave pattern is projected to change little over land, although a slight strengthening occurs over the north Pacific and is more circumglobally (Figure 2b).

Figure 3 shows a lead-lag regression of the first principal component (PC1) of V200 onto other daily anomaly variables to understand the time evolution of the stationary wave and how it impacts fire occurrence. From day −15 to day 0, the midlatitude lower-tropospheric wind at 850 hPa shows a strengthening of the wave pattern that is almost stable or propagates very slow eastward (top panels in Figure 3). This feature is equivalent to the upper-tropospheric pattern shown in Figure 2, where the lower-tropospheric anticyclone (sinking motion) tends to be found downstream from the upper-tropospheric ridge (Holton, 2004). Notably, the lower-tropospheric circulation anomalies over the North America are fairly strong, while those over the Asia are weaker in this analysis. This coupling of monsoon cyclones and anticyclones might also contribute to changes in precipitation and circulation, thus impacting wildfire activity. On day 0, the low-level anticyclone reaches its maximum strength and is centered in the eastern United States, Europe, and central North Asia, where the accompanying fire anomalies indicate a maximum at the west/southward edge of these anticyclones. We note that the centers of the anomalous anticyclone and fire count are shifted around, where the positive fire anomaly occurs along the eastern side of the anticyclone over the Eurasian continent but occurs slightly around the center of the anticyclone over the western North America. By the end of its lifetime, the stationary zonal wavenumber 5–6 pattern is diminished.

The surface relative humidity tends to be lower than normal over the region of anomalous burned area (blue in middle panels in Figure 3), consistent with the early study of Namias (1955) that the high-pressure systems within the stationary wave create dry atmospheric and soil conditions. The strengthening of the anticyclone/high-pressure center at day 0 leads to a deeper intrusion and intensification of subsidence and drying (or ascent and wetting in the low-pressure center). A consistent pattern is found in the soil moisture, with negative anomalies (crossed pattern in Figure 3) generally located over the low relative humidity region. However, we note that some regions, such as the southeastern United States and northern Russia near the Arctic circle, show an anticorrelation between surface relative humidity and soil moisture. This is likely due to the distribution of vegetation and local atmospheric conditions, as well as the lag response of the soil moisture to surface relative humidity (Niu et al., 2018), whereas the latter needs to dry enough to dry out the soil.

Consistent with the stationary wave pattern, the wave-induced variability in precipitation shows an organized pattern. As the sea surface temperature is fully coupled in the model simulations, the associated variation in maximum surface temperature also showed a wave pattern (bottom panels in Figure 3). This structure clearly illustrates that there is a dry heatwave collocated with the stationary wave pattern over the downstream regions of the ridge across the midlatitudes (see also Figure S6 in Supporting Information S1). This result further supports the interpretation that the stationary wave pattern modulates wildfires as well as other extreme weather events on a hemispheric scale in agreement with other local/case studies (e.g., Petoukhov et al., 2018; Teng et al., 2013).

3.2. Linkage Between Persistence of High-Pressure Days and Wildfire

In addition to the impacts of the stationary wave pattern on wildfire activities, here we show that wildfires in midlatitude regions are also modulated by the number of consecutive high-pressure days (Figure 4). Note that we focus on the persistence of descending motion rather than intensity of a high-pressure system. We define a fire occurrence index, which is the ratio between the anomalous fire count associated with the number of high-pressure days (days with vertical descending motion, defined as a positive value of omega at 500 hPa,

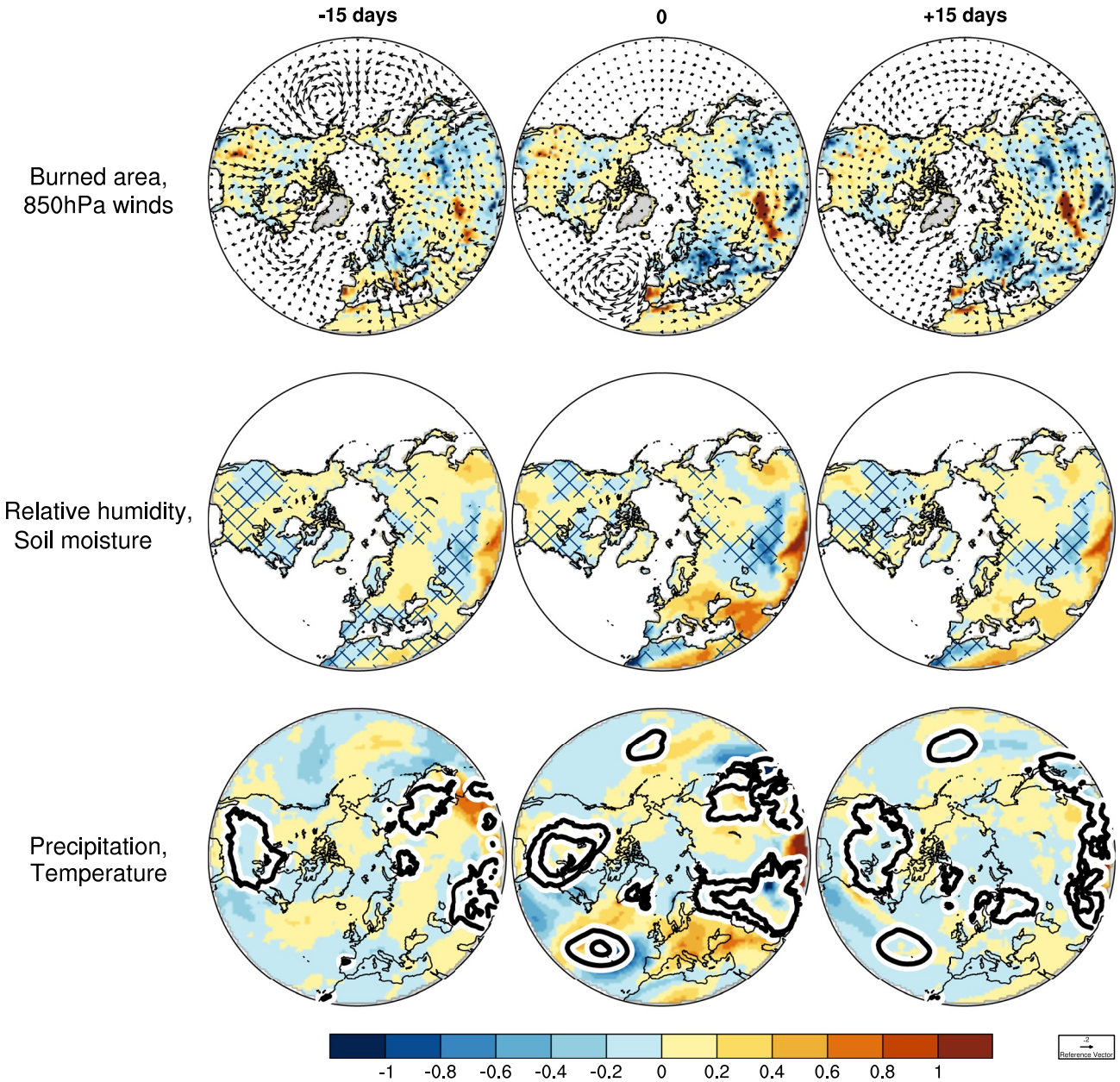

Figure 3. Lead-lag regression maps (−15 days to +15 days) of the PC of stationary waves from the first singular value decomposition (SVD) to the burned area (shaded, units are km^2/year/m/s) and 850 hPa winds (top panels), 2 m relative humidity (shaded, units are %/m/s) and soil moisture (only negative anomaly shown with crossed-pattern, units are kg/m^2/m/s) (middle panels), and precipitation (shaded, units are mm/day/m/s) and surface temperature anomaly (contour, only positive anomaly shown, units are K/m/s, contour interval 0.03, 0.1) (bottom panels) for the historical simulation (1981–2010). Similar plots for the geopotential height at 200 hPa and 850 hPa and the omega at 500 hPa are shown in Figure S6 in Supporting Information S1. Maps corresponding to the SSP370 (2071–2100) simulation are shown in Figure S11 in Supporting Information S1.

$\omega 500 > 0$) and the boreal summer climatological mean of fire count (i.e., fire count$_{\text{(consecutive high-pressure days)}}$/fire$_{\text{mean}}$). The longer the period of high-pressure days, the higher the chance for wildfires to occur (Figure 4a). This feature is consistently shown in the three major fire regions in the United States, southern Europe, and northern Asia, although the amplitude of the fire occurrence index is different (see Figure S7 in Supporting Information S1). In particular, fire count and burned area increase as the consecutive high-pressure days increase up to 10–12 days (Figures 4a and 4b). This increase is due to prolonged periods of low relative humidity and soil moisture with high-pressure days – accompanied by high temperature and no or reduced precipitation (Figure S8 in Supporting Information S1) – that can effectively dry out fuels and thus support wildfire occurrence (F. Chen et al., 2014).

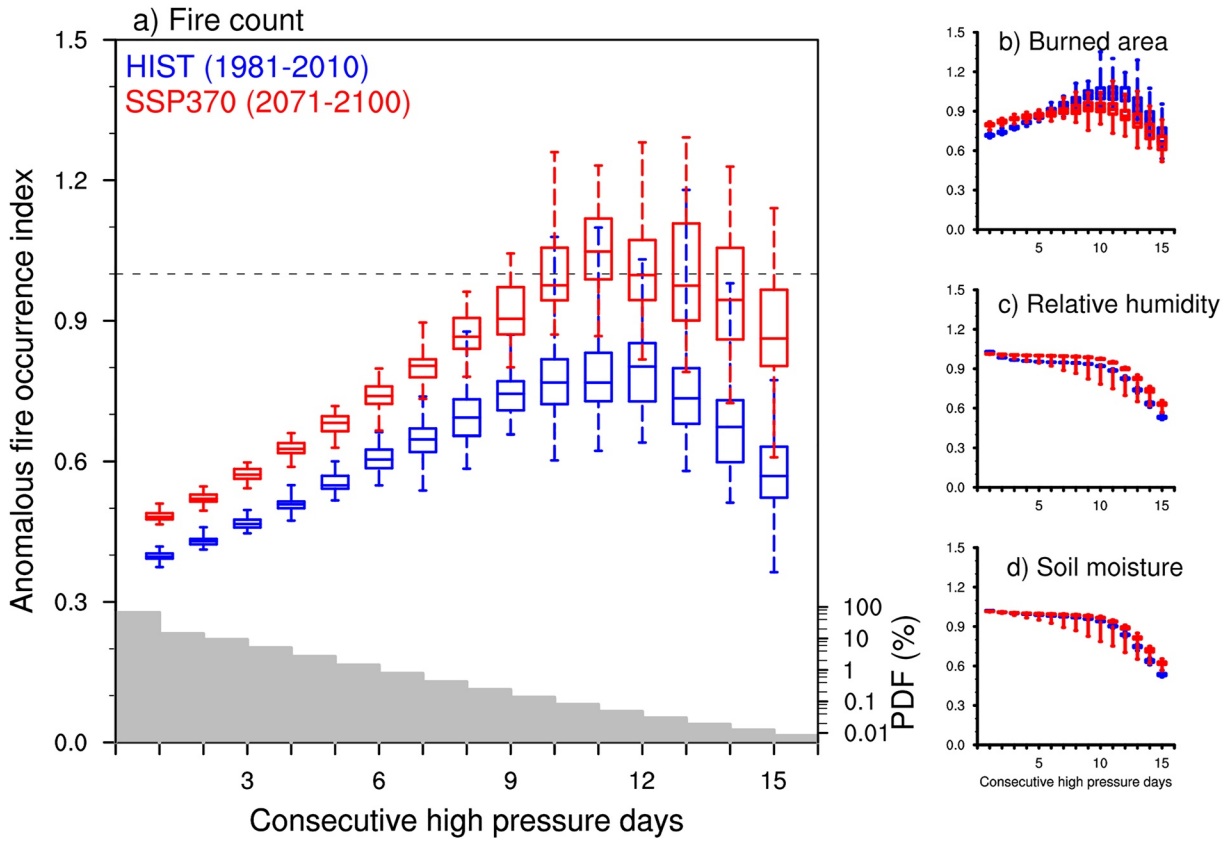

Figure 4. (a) Histograms of the anomalous fire occurrence index, defined as a ratio between anomalous fire count and the boreal summer climatological mean, as a function of the consecutive high-pressure days, defined as days with positive vertical pressure velocity at 500 hPa ($\omega 500 > 0$), for the historical (1981–2010, blue) and SSP370 (2071–2100, red) simulations. On each box, the central bar indicates the median, and the bottom and top edges of the box indicate the 25th and 75th percentiles of 50 ensemble members, respectively. The shaded gray bars (bottom, right *y*-axis on the logarithmic scale) are the ensemble mean probability distribution function (PDF) of frequency of the consecutive high-pressure days in the historical and SSP370 simulation (the PDFs of historical and SSP370 are almost identical). The dashed horizontal line represents the doubling line of anomalous wildfire occurrence compared to the boreal summer climatological mean (b, c, d) Similar to (a) but for the burned area, relative humidity, and soil moisture, respectively. Similar plots for several specific domains as well as variables (e.g., precipitation, surface temperature, and drought index) are shown in Figures S7 and S8 in Supporting Information S1.

It is interesting that the fire occurrence tends to decrease after about the 12th consecutive high-pressure day (Figures 4a and 4b). Given the complication of fire parameterization in climate model and fire behavior in the real climate system, we hesitate to extrapolate our results shown here. Regardless, the decrease of fire may be likely due to loss of fuels by fire on previous high-pressure days (in the real world) and/or the decrease of surface temperature and drought index (Figures S8b and S8c in Supporting Information S1). The accelerated decrease in relative humidity and soil moisture occurs after the maximum fire (day 10–12) might be because of a strong evaporation due to fire exposure. These results deserve to be examined further.

3.3. Responses of Stationary Waves and Wildfires to Future Global Warming

In our current analysis, the ensemble mean of 50 members shows little change in stationary wave patterns over land (Figure 2b), although it shows a more circumglobal pattern – or an increase in stationary zonal wavenumber and/or quasi-resonant amplification (Wills et al., 2019). The uncertainty in the changes in the stationary wave is not necessarily due to competing effects of weakening circulations (Chou et al., 2009) by global energetic constraints, whereby global precipitation increases at a slower rate than tropospheric moisture and strengthening circulations (Hu & Fedorov, 2019) caused by increased latent heat in a warmer climate. Other studies have even suggested an Arctic origin (Coumou et al., 2018; Sato & Nakamura, 2019) for stationary wave changes although the statistical linkages between Arctic sea-ice and midlatitude stationary waves are relatively weak (Screen & Simmonds, 2014).

In contrast to the modest response of stationary waves to global warming, wildfire counts are projected to increase considerably (Figures 2 and 4). Such robust changes occur in both the mean and variability in wildfires, which may arise from more dryness over land due to relative humidity decreases associated with an increase in land-ocean temperature contrast in mid- and high-latitudes that create an arid land surface (Byrne & O'Gorman, 2016; see also Figures S9 and S10 in Supporting Information S1). The increases in evapotranspiration due to overall warmer conditions can also play a role (not shown). The weakening and shifting of storm tracks (Gertler et al., 2020; Lee et al., 2021) and expansion of subtropical high-pressure systems (Lin & Chan, 2015) in response to global warming could also favor the buildup of hot and dry conditions over land, which in turn dry out the soil and potentially increase wildfire occurrence (Figures S9 and S10 in Supporting Information S1). Additionally, fire patterns in the midlatitudes are modulated by high latitude climate modes which have been projected to change with warming (Jain & Flannigan, 2021; Sato & Nakamura, 2019). The projected increase in Arctic lightning might also increase fire risk (Y. Chen et al., 2021), as has been demonstrated within the North American boreal region (Veraverbeke et al., 2017), but this effect is not included in the CESM2. Changes in other tropical modes in response to global warming, such as El Niño/Southern Oscillation (ENSO), would also contribute to the enhancement of wildfires (Fang et al., 2021) and are predicted to be strengthened in the future climate (Cai et al., 2014). Additionally, the expansion and intensification of agriculture as well as the increase in fire suppression management will contribute to the overall smaller area of wildfires, although the fire count will increase in the future climate.

4. Summary and Discussion

We have examined the relationship between stationary waves and wildfires in the midlatitude region during the boreal summer and their projected changes by the end of 21st century in the high emission scenario (SSP370), using 50 simulations from CESM2-LE. The results suggest that the leading mode of stationary wave pattern characterized by zonal wavenumber 5–6 tends to link to wildfire occurrences. Our focus in this study is only on the leading mode but it is noted that many fires in the real climate system have occurred under different wave pattern regimes, such as zonal wavenumber 4 pattern occurring in the 2016 Alberta wildfire (Petoukhov et al., 2018). Fires over North America also show a complicated connection with the atmospheric pattern (Crimmins, 2006; Lindley et al., 2017). Therefore, questions remain as to why stationary wave and wildfire activity variations do not show a similar phase relationship in every region, whether this discrepancy is also presented to other climate models, whether the difference is partially due to unique region characteristics that regulate wildfires, or whether our current understanding of wildfire occurrence is complete. More work is needed to understand the relationship between stationary wave patterns and wildfire occurrence, in particular, how changes in the vertical and horizontal structures of waves mediate this relationship, including teleconnections.

Under global warming, Figure 2 suggests that factors other than changes in stationary wave patterns alone are responsible for the increase in wildfires since the change in wave patterns over land is very small. This result is also supported by the probability distribution (frequency of occurrence) function of consecutive high-pressure days in Figure 4, which shows almost no change between the current and future climates. Admittedly, the coherent structures between the upper-level circulation anomaly and wildfire activities are not complete given the complexity of fire behavior and atmosphere-land interaction processes. Hence, further work using other datasets is necessary to affirm the validity of our results, to provide more confidence in the synchronization between atmospheric wave and extreme events such as wildfires. The fire parameterizations in land models also remain an outstanding area for improvement for climate model simulations (Fisher & Koven, 2020; Friedingstein et al., 2014), but our results suggest that fire occurrence can be linked to global-scale modes of atmospheric variability that may afford opportunities to improve wildfire forecasts.

Data Availability Statement

The CESM2-LE outputs are available at https://www.cesm.ucar.edu/projects/community-projects/LENS2/data-sets.html. The fire emission data can be retrieved from the Global Fire Emission Database at https://www.geo.vu.nl/~gwerf/GFED/GFED4/. The ERA5 Fire Weather Index (FWI) and wind are obtained from the ECMWF website at https://doi.org/10.24381/cds.0e89c522 and https://doi.org/10.24381/cds.bd0915c6, respectively. A NCL code to calculate the fire weather index from CESM2-LE is available online at https://github.com/NCAR/fire-indices.

Acknowledgments
This work was supported by the Institute for Basic Science (IBS), Republic of Korea, under IBS-R028-D1. The data analysis and calculations were conducted on the IBS/ICCP supercomputer Aleph (with 1.43-petaflop high-performance Cray XC50-LC Skylake computing system with 18,720 processor cores, 9.59-petabyte storage, and 43-petabyte tape archive space). H.X.B was also supported by Australian Research Council (ARC) under grant CE170100023. E.D.M was supported by the Climate and Large-Scale Dynamics program of the National Science Foundation under grant AGS-1841754. W.R.W is supported by the National Center for Atmospheric Research, which is a major facility sponsored by the National Science Foundation under Cooperative Agreement No. 1852977. We thank two anonymous reviewers for insightful comments that helped improve the manuscript. We thank all the scientists, software engineers, and administrators who contributes to the development of CESM2-LE.

References

Branstator, G. (2002). Circumglobal teleconnections, the jet stream waveguide, and the North Atlantic Oscillation. *Journal of Climate*, *15*(14), 1893–1910. https://doi.org/10.1175/1520-0442(2002)015<1893:cttjsw>2.0.co;2

Brey, S. J., Barnes, E. A., Pierce, J. R., Swann, A. L. S., & Fischer, E. V. (2021). Past variance and future projections of the environmental conditions driving Western U.S. summertime wildfire burn area. *Earth's Future*, *9*(2), e2020EF001645. https://doi.org/10.1029/2020EF001645

Byrne, M. P., & O'Gorman, P. A. (2015). The response of precipitation minus evapotranspiration to climate warming: Why the "wet-get-wetter, dry-get-drier" scaling does not hold over land. *Journal of Climate*, *28*(20), 8078–8092. https://doi.org/10.1175/jcli-d-15-0369.1

Byrne, M. P., & O'Gorman, P. A. (2016). Understanding decreases in land relative humidity with global warming: Conceptual model and GCM simulations. *Journal of Climate*, *29*(24), 9045–9061. https://doi.org/10.1175/jcli-d-16-0351.1

Cai, W., Borlace, S., Lengaigne, M., van Rensch, P., Collins, M., Vecchi, G., et al. (2014). Increasing frequency of extreme El Niño events due to greenhouse warming. *Nature Climate Change*, *4*(2), 111–116. https://doi.org/10.1038/nclimate2100

Chen, F., Fan, Z., Niu, S., & Zheng, J. (2014). The influence of precipitation and consecutive dry days on burned areas in Yunnan Province, Southwestern China. *Advances in Meteorology*, 1–11. https://doi.org/10.1155/2014/748923

Chen, Y., Romps, D. M., Seeley, J. T., Veraverbeke, S., Riley, W. J., Mekonnen, Z. A., & Randerson, J. T. (2021). Future increases in Arctic lightning and fire risk for permafrost carbon. *Nature Climate Change*, *11*(5), 404–410. https://doi.org/10.1038/s41558-021-01011-y

Chou, C., Neelin, J. D., Chen, C. A., & Tu, J. Y. (2009). Evaluating the rich-get-richer mechanism in tropical precipitation change under global warming. *Journal of Climate*, *22*(8), 1982–2005. https://doi.org/10.1175/2008JCLI2471.1

Conard, S., & Ponomarev, E. (2020). *Fire in the North – The 2020 Siberian fire season*. Wildfire.

Coumou, D., Di Capua, G., Vavrus, S., Wang, L., & Wang, S. (2018). The influence of Arctic amplification on mid-latitude summer circulation. *Nature Communications*, *9*(1), 2959. https://doi.org/10.1038/s41467-018-05256-8

Coumou, D., Petoukhov, V., Rahmstorf, S., Petri, S., & Schellnhuber, H. J. (2014). Quasi-resonant circulation regimes and hemispheric synchronization of extreme weather in boreal summer. *Proceedings of the National Academy of Sciences*, *111*(34), 12331–12336. https://doi.org/10.1073/pnas.1412797111

Crimmins, M. A. (2006). Synoptic climatology of extreme fire-weather conditions across the southwest United States. *International Journal of Climatology: A Journal of the Royal Meteorological Society*, *26*(8), 1001–1016. https://doi.org/10.1002/joc.1300

Danabasoglu, G., Lamarque, J.-F., Bacmeister, J., Bailey, D. A., DuVivier, A. K., Edwards, J., et al. (2020). The Community Earth System model version 2 (CESM2). *Journal of Advances in Modeling Earth Systems*, *12*(2), e2019MS001916. https://doi.org/10.1029/2019MS001916

Davies, L., Jakob, C., May, P., Kumar, V. V., & Xie, S. (2013). Relationships between the large-scale atmosphere and the small-scale convective state for Darwin, Australia. *Journal of Geophysical Research: Atmospheres*, *118*(20), 11534–11545. https://doi.org/10.1002/jgrd.50645

Ding, Q., & Wang, B. (2005). Circumglobal teleconnection in the Northern Hemisphere summer. *Journal of Climate*, *18*(17), 3483–3505. https://doi.org/10.1175/jcli3473.1

Edwards, D. P., Emmons, L. K., Hauglustaine, D. A., Chu, D. A., Gille, J. C., Kaufman, Y. J., et al. (2004). Observations of carbon monoxide and aerosols from the Terra satellite: Northern Hemisphere variability. *Journal of Geophysical Research*, *109*, D24. https://doi.org/10.1029/2004JD004727

Fang, K., Yao, Q., Guo, Z., Zheng, B., Du, J., Qi, F., et al. (2021). ENSO modulates wildfire activity in China. *Nature Communications*, *12*(1), 1764. https://doi.org/10.1038/s41467-021-21988-6

Fisher, R. A., & Koven, C. D. (2020). Perspectives on the future of land surface models and the challenges of representing complex terrestrial systems. *Journal of Advances in Modeling Earth Systems*, *12*(4), e2018MS001453. https://doi.org/10.1029/2018MS001453

Friedingstein, P., Meinshausen, M., Arora, V. K., Jones, C. D., Anav, A., Liddicoat, S. K., & Knutti, R. (2014). Uncertainties in CMIP5 climate projections due to carbon cycle feedbacks. *Journal of Climate*, *27*(2), 511–526. https://doi.org/10.1175/jcli-d-12-00579.1

Gertler, C. G., O'Gorman, P. A., Kravitz, B., Moore, J. C., Phipps, S. J., & Watanabe, S. (2020). Weakening of the extratropical storm tracks in solar geoengineering scenarios. *Geophysical Research Letters*, *47*(11), e2020GL087348. https://doi.org/10.1029/2020GL087348

Giglio, L., Randerson, J. T., & Van Der Werf, G. R. (2013). Analysis of daily, monthly, and annual burned area using the fourth-generation global fire emissions database (GFED4). *Journal of Geophysical Research: Biogeosciences*, *118*(1), 317–328. https://doi.org/10.1002/jgrg.20042

Hantson, S., Kelley, D. I., Arneth, A., Harrison, S. P., Archibald, S., Bachelet, D., et al. (2020). Quantitative assessment of fire and vegetation properties in simulations with fire-enabled vegetation models from the Fire Model Intercomparison Project. *Geoscientific Model Development*, *13*(7), 3299–3318. https://doi.org/10.5194/gmd-13-3299-2020

Haugen, M. A., Stein, M. L., Moyer, E. J., & Sriver, R. L. (2018). Estimating changes in temperature distributions in a large ensemble of climate simulations using quantile regression. *Journal of Climate*, *31*(20), 8573–8588. https://doi.org/10.1175/jcli-d-17-0782.1

Held, I. M., Ting, M., & Wang, H. (2002). Northern winter stationary waves: Theory and modeling. *Journal of Climate*, *15*(16), 2125–2144. https://doi.org/10.1175/1520-0442(2002)015<2125:nwswta>2.0.co;2

Hersbach, H., Bell, B., Berrisford, P., Hirahara, S., Horányi, A., Mucoz-Sabater, J., et al. (2020). The ERA5 global reanalysis. *Quarterly Journal of the Royal Meteorological Society*, *146*(730), 1999–2049. https://doi.org/10.1002/qj.3803

Holton, J. (2004). *An introduction to dynamic meteorology* (4th ed., pp. 1–535). Academic Press.

Hu, S., & Fedorov, A. V. (2019). Indian Ocean warming can strengthen the Atlantic meridional overturning circulation. *Nature Climate Change*, *9*(10), 747–751. https://doi.org/10.1038/s41558-019-0566-x

Jain, P., & Flannigan, M. (2021). The relationship between the polar jet stream and extreme wildfire events in North America. *Journal of Climate*, *34*(15), 6247–6265. https://doi.org/10.1175/jcli-d-20-0863.1

Kornhuber, K., Coumou, D., Vogel, E., Corey, L., Donges, J. F., Lehmann, J., & Horton, R. M. (2020). Amplified rossby waves enhance risk of concurrent heatwaves in major breadbasket regions. *Nature Climate Change*, *10*(1), 48–53. https://doi.org/10.1038/s41558-019-0637-z

Kornhuber, K., Scott, O., Coumou, D., Petri, S., Petoukhov, V., Grey, L., & Gray, L. (2019). Extreme weather events in early summer 2018 connected by a recurrent hemispheric wave-7 pattern. *Environmental Research Letters*, *14*(5), 054002. https://doi.org/10.1088/1748-9326/ab13bf

Lagouvardos, K., Kotroni, V., Giannaros, T. M., & Dafis, S. (2018). Meteorological conditions conducive to the rapid spread of the deadly wildfire in Eastern Attica, Greece. *Bulletin of the American Meteorological Society*, *100*(11), 2137–2145. https://doi.org/10.1175/bams-d-18-0231.1

Lawrence, D. M., Fisher, R. A., Koven, C. D., Oleson, K. W., Swenson, S. C., Bonan, G., et al. (2019). The Community Land Model version 5: Description of new features, benchmarking, and impact of forcing uncertainty. *Journal of Advances in Modeling Earth Systems*, *11*(12), 4245–4287. https://doi.org/10.1029/2018MS001583

Lee, J.-Y., Marotzke, J., Bala, G., Cao, L., Corti, S., Dunee, J. P., et al. (2021). Future global climate: Scenario-based projections and near-term information. In climate change 2021: Future global climate: Scenario-based projections and near-term information. In V. Masson-Delmotte, P. Zhai, A. Pirani, S. L. Connors, C. Péan, S. Berger, et al., (Eds.), *Climate change 2021: The physical science basis. Contribution of working*

group I to the sixth assessment report of the intergovernmental panel on climate change (pp. 553–672). Cambridge University Press. https://doi.org/10.1017/9781009157896.006

Li, F., & Lawrence, D. M. (2017). Role of fire in the global land water budget during the twentieth century due to changing ecosystems. *Journal of Climate*, *30*(6), 1893–1908. https://doi.org/10.1175/jcli-d-16-0460.1

Lin, I.-I., & Chan, J. C. L. (2015). Recent decrease in typhoon destructive potential and global warming implications. *Nature Communications*, *6*(1), 7182. https://doi.org/10.1038/ncomms8182

Lindley, T., Bowers, B. R., Murdoch, G. P., Smith, B. R., & Gitro, C. M. (2017). Fire-effective low-level thermal ridges on the southern Great Plains. *Journal of Operational Meteorology*, *5*(12), 146–160. https://doi.org/10.15191/nwajom.2017.0512

Nakamura, H., Nakamura, M., & Anderson, J. L. (1997). The role of high-and low-frequency dynamics in blocking formation. *Monthly Weather Review*, *125*(9), 2074–2093. https://doi.org/10.1175/1520-0493(1997)125<2074:trohal>2.0.co;2

Namias, J. (1955). Some meteorological aspects of drought. *Monthly Weather Review*, *83*(9), 199–205. https://doi.org/10.1175/1520-0493(1955)083<0199:smaod>2.0.co;2

Niu, J., Chen, J., Sun, L., & Sivakumar, B. (2018). Time-lag effects of vegetation responses to soil moisture evolution: A case study in the Xijiang basin in South China. *Stochastic Environmental Research and Risk Assessment*, *32*(8), 2423–2432. https://doi.org/10.1007/s00477-017-1492-y

O'Neill, B. C., Tebaldi, C., Vuuren, D. P. V., Eyring, V., Friedlingstein, P., Hurtt, G., et al. (2016). The scenario model intercomparison project (ScenarioMIP) for CMIP6. *Geoscientific Model Development*, *9*(9), 3461–3482. https://doi.org/10.5194/gmd-9-3461-2016

Petoukhov, V., Petri, S., Kornhuber, K., Thonicke, K., Coumou, D., & Schellnhuber, H. J. (2018). Alberta wildfire 2016: Apt contribution from anomalous planetary wave dynamics. *Scientific Reports*, *8*(1), 12375. https://doi.org/10.1038/s41598-018-30812-z

Petoukhov, V., Rahmstorf, S., Petri, S., & Schellnhuber, H. J. (2013). Quasiresonant amplification of planetary waves and recent Northern Hemisphere weather extremes. *Proceedings of the National Academy of Sciences*, *110*(14), 5336–5341. https://doi.org/10.1073/pnas.1222000110

Rabin, S. S., Melton, J. R., Lasslop, G., Bachelet, D., Forrest, M., Hantson, S., et al. (2017). The fire modeling intercomparison project (FireMIP), phase 1: Experimental and analytical protocols with detailed model descriptions. *Geoscientific Model Development*, *10*(3), 1175–1197. https://doi.org/10.5194/gmd-10-1175-2017

Rodgers, K. B., Lee, S.-S., Rosenbloom, N., Timmermann, A., Danabasoglu, G., Deser, C., et al. (2021). Ubiquity of human-induced changes in climate variability. *Earth System Dynamics*, *12*(4), 1393–1411. https://doi.org/10.5194/esd-12-1393-2021

Rohini, P., Rajeevan, M., & Srivastava, A. (2016). On the variability and increasing trends of heat waves over India. *Scientific Reports*, *6*(1), 26153. https://doi.org/10.1038/srep26153

Ruffault, J., Curt, T., Moron, V., Trigo, R. M., Mouillot, F., Koutsias, N., et al. (2020). Increased likelihood of heat-induced large wildfires in the Mediterranean Basin. *Scientific Reports*, *10*(1), 13790. https://doi.org/10.1038/s41598-020-70069-z

Sato, T., & Nakamura, T. (2019). Intensification of hot Eurasian summers by climate change and land-atmosphere interactions. *Scientific Reports*, *9*(1), 10866. https://doi.org/10.1038/s41598-019-47291-5

Schulze, S. S., Fischer, E. C., Hamideh, S., & Mahmoud, H. (2020). Wildfire impacts on schools and hospitals following the 2018 California Camp Fire. *Natural Hazards*, *104*(1), 901–925. https://doi.org/10.1007/s11069-020-04197-0

Screen, J. A., & Simmonds, I. (2014). Amplified mid-latitude planetary waves favour particular regional weather extremes. *Nature Climate Change*, *4*(8), 704–709. https://doi.org/10.1038/nclimate2271

Shaw, T., & Voigt, A. (2015). Tug of war on summertime circulation between radiative forcing and sea surface warming. *Nature Geoscience*, *8*(7), 560–566. https://doi.org/10.1038/ngeo2449

Shukla, P., Skea, J., Calvo Buendia, E., Masson-Delmotte, V., Pɒrtner, H., Roberts, D., et al. (2019). Climate change and land: An IPCC special report on climate change, desertification, land degradation, sustainable land management, food security, and greenhouse gas fluxes in terrestrial ecosystems.

Teng, H., Branstator, G., Wang, H., Meehl, G. A., & Washington, W. M. (2013). Probability of US heat waves affected by a subseasonal planetary wave pattern. *Nature Geoscience*, *6*(12), 1056–1061. https://doi.org/10.1038/ngeo1988

Valendik, E., Kisilyakhov, E., Ryzhkova, V., Ponomarev, E., & Danilova, I. (2014). Conflagration fires in taiga landscapes of Central Siberia. *Geography and Natural Resources*, *35*(1), 41–47. https://doi.org/10.1134/S1875372814010065

Van der Werf, G., Randerson, J. T., Giglio, L., van Leeuwen, T. T., Chen, Y., Rogers, B. M., et al. (2017). Global fire emissions estimates during 1997-2016. *Earth System Science Data*, *9*(2), 697–720. https://doi.org/10.5194/essd-9-697-2017

Van Wagner, C. E., & Pickett, T. L. (1985). *Equations and FORTRAN program for the Canadian forest fire weather index system*. Forestry Technical Report 33. Canadian Forest Service.

Veraverbeke, S., Rogers, B. M., Goulden, M. L., Jandt, R. R., Miller, C. E., Wiggins, E. B., & Randerson, J. T. (2017). Lightning as a major driver of recent large fire years in North American boreal forests. *Nature Climate Change*, *7*(7), 529–534. https://doi.org/10.1038/nclimate3329

Wallace, J. M., Smith, C., & Bretherton, C. S. (1992). Singular value decomposition of wintertime sea surface temperature and 500-mb height anomalies. *Journal of Climate*, *5*(6), 561–576. https://doi.org/10.1175/1520-0442(1992)005<0561:svdows>2.0.co;2

Wills, R. C. J., White, R. H., & Levine, X. J. (2019). Northern hemisphere stationary waves in a changing climate. *Current Climate Change Reports*, *5*(4), 372–389. https://doi.org/10.1007/s40641-019-00147-6

Wirth, V., & Polster, C. (2021). The problem of diagnosing jet waveguidability in the presence of large-amplitude eddies. *Journal of the Atmospheric Sciences*, *78*(10), 3137–3151. https://doi.org/10.1175/jas-d-20-0292.1

Wolf, G., Brayshaw, D. J., Klingaman, N. P., & Czaja, A. (2018). Quasi-stationary waves and their impact on European weather and extreme events. *Quarterly Journal of the Royal Meteorological Society*, *144*(717), 2431–2448. https://doi.org/10.1002/qj.3310